RSC Advances




ROYAL SOCIETY OF CHEMISTRY

www.rsc.org/advances

Journal Name

ARTICLE

# Chemically Integrated Hierarchical Hybrid Zinc Cobaltate/Reduced Graphene Oxide Microsphere as Enhanced Lithium-Ion Battery Anode†

Chang Chen,[a,‡] Borui Liu,[d,‡] Qiang Ru,[a,b,c,‡,*] Shaomeng Ma,[a] Shejun Hu,[a,b,c] Xianhua Hou,[a,b,c]

Received 00th January 20xx,
Accepted 00th January 20xx

DOI: 10.1039/x0xx00000x

www.rsc.org/

Chemically integrated hierarchical microsphere $ZnCo_2O_4$/reduced graphene oxide hybrid composites are synthesized via a polyol process. Microsphere $ZnCo_2O_4$ particles embedded in graphene homogeneously with a size region of 320-512 nm, graphene sheets grew and interwoven in the inside of microsphere $ZnCo_2O_4$ particles in inverse, possessing a unique microsphere-sheet hybrid structure. The interconnected graphene conductive network basic skeleton is beneficial to the transportation of $Li^+$ and electrons. Compared with the conventional combination way of metal oxides and graphene, hierarchical microsphere $ZnCo_2O_4$/reduced graphene oxide hybrid composites exhibit enhanced rate capability (469.7 mAh $g^{-1}$ at 4000 mA $g^{-1}$) and long term cycling ability with high capability (904.2 mAh $g^{-1}$ at 1000 mA $g^{-1}$ over 500 charge/discharge cycles), owing to the special characteristic of three-dimensional structure. Most importantly, with the successful synthesis of the hierarchical microsphere $ZnCo_2O_4$/reduced graphene oxide hybrid composites, this facile strategy can extend to synthesize the ternary transition metal oxides/reduced graphene oxide with hierarchical microsphere structure and make it possible to explore more promising storage application.

## Introduction

In recent decades, with the growing energy consumption demands and the development of the energy conversion, the applications of lithium-ion batteries (LIBs) with high efficiency and high energy density are receiving increasingly attention.[1-3] Recently, owing to the low specific capacity and poor rate capacity, the commercial graphite carbon anode (372 mAh $g^{-1}$) hinders the further development of lithium-ion batteries.[4] Currently, the binary and ternary transition metal oxide anodes TMOs (T= Zn, Co, Fe, Mn, M= Co, Sn, Fe) have been regarded as promising anode materials due to their high theoretical capacity, such as $Fe_3O_4$ ,[5-6] $Co_3O_4$,[7] NiO,[8-9] $Co_2SnO_4$,[10-11] $ZnMn_2O_4$[12] and $CuCo_2O_4$,[13] which have been used as anode materials to improve the capacity of LIBs in the last decades. Those transition metal oxide anodes have drawn particular attention because of their high theoretical capacity, high abundance and high corrosion resistance. However, those TMOs anodes always suffer from detrimental structural collapse, large volume expansion, inferior rate capability and electrode cracking, leading to poor cycling stability and low power densities during the charge/discharge process.[14-17]

Tremendous efforts have recently been made to tackle those intractable issues, such as element doping, carbon based composites, nanostructure constructions and compounding metal oxides. As a two dimensional atomic sheets of $sp^2$ carbon atoms, graphene has attracted keen interest since discovered in 2004.[18-20] The theoretical graphene sheets possess much especial properties, for instance, owing to its large surface area, high electron conductivity (~15,000 $cm^2$ $V^{-1}$ $s^{-1}$ at 300 K and 60,000 $cm^2$ $V^{-1}$ $s^{-1}$ at 4 K), chemical stability and planar $sp^2$ hybridized carbon framework.[20,21-22] Thus, graphene is usually selected as a based good conductive network and the strategy of preparing TMOs/graphene composites may be an effective way to gain anode materials with improved electrochemical performance.[23-25]

*a Laboratory of Quantum Engineering and Quantum Materials, School of Physics and Telecommunication Engineering, South China Normal University, Guangzhou 510006, PR China.*

*b Guangdong Engineering Technology Research Center of Efficient Green Energy and Environment Protection Materials, Guangzhou 510631, PR China.*

*c Engineering Research Center of Materials and Technology for Electrochemical Energy Storage (Ministry of Education), Guangzhou 510006, PR China.*

*d Department of Mechanical Engineering, University of Texas at Austin, Austin, TX 78712, United States.*

**Corresponding author: Email: rq7702@yeah.net, Tel: +86-20-39310066, (Q. Ru).*

*‡ These authors contributed equally to this work.*

*Electronic Supplementary Information (ESI) available: [details of any supplementary information available should be included here]. See DOI: 10.1039/x0xx00000x*

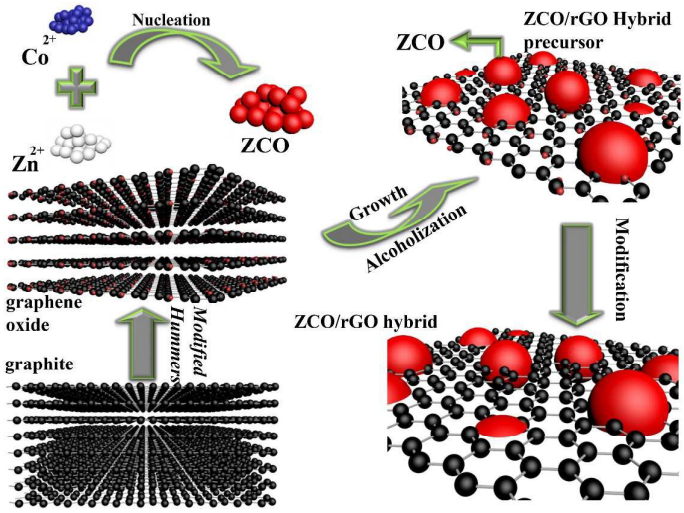


**Fig.1.** Schematic diagram for the preparation process of ZCO/rGO hybrid composites.

As anode materials, $ZnCo_2O_4$ (ZCO) have received special attention, which is ascribed to their unique crystalline structure and remarkable electrochemical reaction mechanism.[26] In the cubic spinel $ZnCo_2O_4$, the $Zn^{2+}$ holds the tetrahedral sites and the $Co^{3+}$ holds the octahedral sites, and the special structure possessing good electrical conductivity can significantly improve its electrochemical performance.[27-28] Liu et al. synthesized $ZnCo_2O_4$ nanorod via hydrothermal method, which exhibited high initial capacity (1509 mAh $g^{-1}$) and good electrochemical cycling performance (767.15 mAh $g^{-1}$ after 50 cycles).[29] Hao et al. presented flower-like multimodal porous $ZnCo_2O_4$ microspheres with high reversible capacity (940 mAh $g^{-1}$ at the current density of 0.1 C and 919 mAh $g^{-1}$ at the current density of 0.2 C after 100 cycles).[30] Wu et al. reported highly symmetric $Zn_xCo_{3-x}O_4$ hollow polyhedral with an excellent reversible capacity (990 mAh $g^{-1}$ after 50 cycles).[31] Whereas, those special structure of $ZnCo_2O_4$ as anode materials are not satisfied, and still need further improvement to meet the demand of high power electric vehicle and large scale electric grids.

In this work, we have proposed a facile synthesis method of involving a polyol process, followed by thermal annealing process for the synthesis of hierarchical microsphere $ZnCo_2O_4$, which has been embedded in reduced graphene oxide and graphene sheet interwoven in $ZnCo_2O_4$ particles to form hierarchical hybrid $ZnCo_2O_4$/reduced graphene oxide microsphere microstructure (ZCO/rGO hybrid ) (Fig. 1). Owing to the special structure, ZCO/rGO hybrid electrodes exhibit enhanced rate capability and good cycling stability of ~904.2 mAh $g^{-1}$ at the current density of 1000 mA $g^{-1}$ after 500 cycles, meanwhile good cycling stability and enhanced electrochemical rate capability.

## Results and discussion

**Synthesis and characterization of ZCO/rGO hybrid composites.**

The XRD patterns are used to identify the phase formation of the individual constituents. The crystallographic structure and phase purity of as-prepared ZCO materials and ZCO/rGO hybrid composites are shown in Fig. 2a. According to the above diffraction pattern, XRD analysis of ZCO/rGO hybrid composites indicates crystalline $ZnCo_2O_4$ particles with a cubic spinel phase (JCPDS NO. 23-1390).[32] A weak peak at 24° can be ascribed to the (002) plane of reduced graphene oxide.[33] The acute diffraction peaks, especially for (311), (220), (511) and (440) planes, declare that ZCO materials and ZCO/rGO hybrid composites are highly crystallized, which is also consistent with standard cubic spinel phase of $ZnCo_2O_4$. As can be seen from the inset of Fig. 2a, after embedded in graphene sheets, the diffraction peaks of

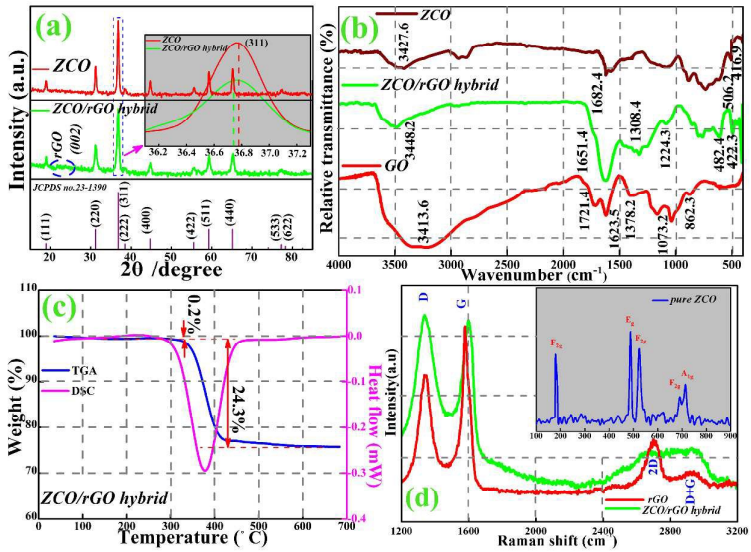


**Fig. 2.** (a) XRD patterns of ZCO materials and ZCO/rGO hybrid composites. The inset of Fig. 2a: the partial enlarged pattern of (311) lattice plane between ZCO materials and ZCO/rGO hybrid composites; (b) FT-IR spectra of ZCO materials, ZCO/rGO hybrid composites and GO materials; (c) TGA-DSC curves of ZCO/rGO hybrid composites tested; (d) Raman spectra of ZCO/rGO hybrid composites.

ZCO/rGO hybrid composites become subtly broaden, which involves the theory of grain refinement.[34-35] In the process of recombine with graphene sheets, the degree of crystallization of ZCO is reduced, and the grain size of ZCO/rGO hybrid composites are smaller than ZCO materials, which alters the width of diffraction peak. Besides, no obvious diffraction peak for impurities is observed, displaying the high purity for both ZCO materials and ZCO/rGO hybrid composites.

FT-IR analysis is applied to identify the presence of numerous functional groups of graphene oxide (GO) materials and ZCO/rGO hybrid composites, such as carbonyl (C=O), carboxyl (-COOH), hydroxyl (-OH), as well as oxygen epoxide groups (bridging oxygen atoms).[36-37] ZCO materials display the vibration mode of Zn-O bond and Co-O bond in the cubic spinel $ZnCo_2O_4$.[38] The FT-IR spectra is given in Fig. 2b over the range of 4000-400 $cm^{-1}$. For GO materials, the strong and broad band for intermolecular hydrogen bonds at 3413.6 $cm^{-1}$ is assigned to the surface –OH vibration of surface carbocyclic rings and the –OH symmetric stretching vibration of absorbed water molecules. The bands at 1623.5 $cm^{-1}$ and 1224.3 $cm^{-1}$ are ascribed to the vibration of C=O and C-O, which indwell in the GO surface. The symmetrical and acute band at 1623.5 $cm^{-1}$ is assigned to C=C skeleton vibration, epoxide groups stretching vibration and –OH bending vibration. Those functional groups vibration demonstrate that GO materials are in abundance with carboxyl, epoxide and hydrophilic groups, which are consistent with the theoretical value.

Furthermore, comparing the FT-IR spectra of ZCO/rGO hybrid composites with GO materials, the above absorption bands diminish or perhaps disappear obviously, manifesting the successful reduction of graphene oxide to reduced graphene oxide. For bare ZCO materials and ZCO/rGO hybrid composites, the especial absorption functional groups are located at 422.3 $cm^{-1}$ and 482.4 $cm^{-1}$. The absorption band at 422.3 $cm^{-1}$ is attributed to the stretching vibration of Co-O bond and the transparent absorption band at 482.4 $cm^{-1}$ is ascribed to the asymmetric vibration of Zn-O bond in the cubic spinel $ZnCo_2O_4$.[20,36-38] Thus, the FT-IR spectra demonstrate that the reduction of graphene oxide to reduced graphene oxide is perfect and the bare ZCO particles are anchored on the surface of graphene sheets during the synthesis. TGA is used to determine the carbon content in ZCO/rGO hybrid composites. Fig. 2c shows the TGA-DSC curves in flowing air atmosphere at the range of 20-680 °C. A weight loss before 100 ºC is ascribed to the evaporation of the residual water, anchoring on the surface of graphene sheets. A weight loss between 100 and 650 °C is due to the removal of the residual oxygen containing functional groups and the combustion of the carbon containing functional groups in ZCO/rGO hybrid composites, and a major evident endothermic peak appears in the corresponding DSC curve. The mass ratio of ZCO: rGO in ZCO/rGO hybrid composites determined by thermal gravimetric analysis (TGA) is close to 3:1.

The Raman spectrum is recorded to further clarify the structure characteristics of rGO materials, pure ZCO materials and ZCO/rGO hybrid composites. A typical Raman spectra is shown in Fig. 2d. As can be seen in the figure, the Raman spectrum of pure ZCO materials shows three types of Raman active bands ($A_{1g}$, $E_g$ and $F_{2g}$). The strong peaks can be found at 692.4 $cm^{-1}$, 608.9 $cm^{-1}$ and 514.2 $cm^{-1}$, 473.1 $cm^{-1}$ and 187.2 $cm^{-1}$, which can be defined as $A_{1g}$, $F_{2g}$ and $F_{2g}$, $E_g$ and $F_{2g}$, respectively.[39-40] Those Raman bands are well in consistent with the reported for the crystalline $ZnCo_2O_4$. Then rGO materials and ZCO/rGO hybrids composites display a highly similar curves. Those two samples display two prominent peaks at 1337.5 $cm^{-1}$ (D band) and 1600.4 $cm^{-1}$ (G band). The D band is due to the breathing mode of k–point phonons of $A_{1g}$ symmetry, which is assigned to the disordered aromatic structure of the $sp^3$ bond carbons. Meanwhile, the G band is related to the first order scattering of the stretching vibration of $sp^2$ carbon atoms, concerning a doubly degenerate phonon mode ($E_{2g}$ symmetry) at the Brillouin zone center that is Raman active for $sp^2$ carbon networks. The peak at 2685.8 $cm^{-1}$ is associated with 2D band and the peak at 2928.8 $cm^{-1}$ is known as the (D+G) band. The 2D band is made by the two phonons double resonance Raman process, which is generated in the second order Raman spectra of graphene without any kind of defect and disorder. The (D+G) band is attributed to a certain extent of disorder of graphene.[41-43] Furthermore, in the process of composited with rGO nanosheets, the degree of Raman peaks of

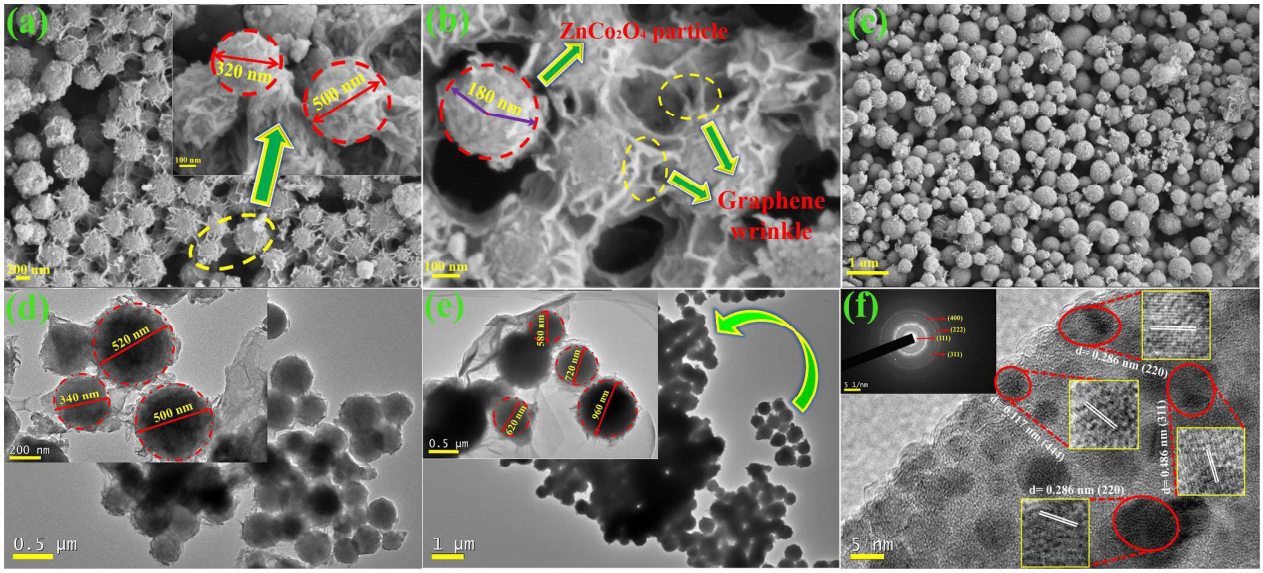


**Fig.3.** (a&b) Scanning electron microscopy (SEM) image of ZCO/rGO hybrid composites. Scale bar, a (200 nm, the inset scale bar is 100 nm) and b (100 nm); (c) SEM image of the mechanical mixed ZCO-G composites. Scale bar, (1 um); (d) TEM image of ZCO/rGO hybrid composites. Scale bar, c (0.5 um, the inset scale bar is 200 nm); (e) TEM image of the mechanical mixed ZCO-G composites. Scale bar, (1um, the inset scale bar is 0.5 um); (f) High-resolution TEM images of ZCO/rGO hybrid composites. Scale bar, (5nm, the inset scale bar is 5 1/nm).

pure ZCO materials is diminished.

The morphology and the structure of the resulting samples are observed by SEM micrographs. As can be seen from Fig. 3a and b, graphene sheets display a structure of curled, wrinkled and irregular to form a 3D network, hierarchical microsphere $ZnCo_2O_4$ are uniformly embedded in curled graphene sheets, the microsphere size varies between 320 and 500 nm, microsphere ZCO particles are dispersed among the entangled graphene sheets randomly. Fig. 3c shows SEM of the mechanical mixed ZCO-G composites. ZCO particles display a micro sized sphere and the diameter is

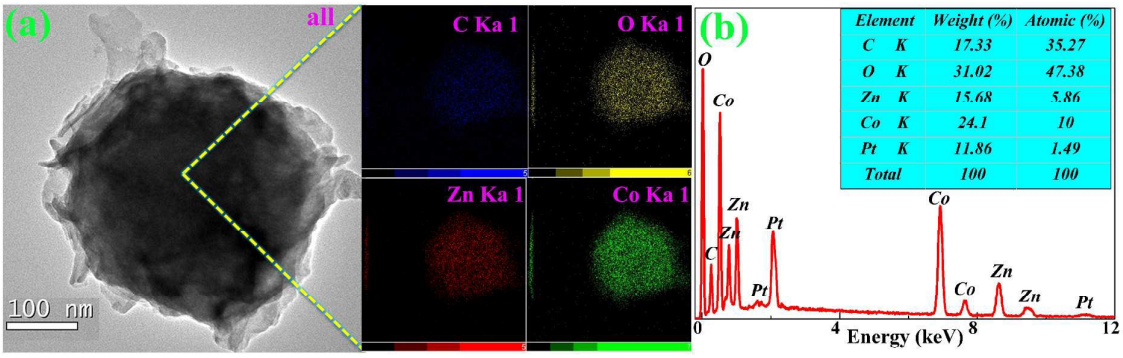


**Fig. 4.** (a) TEM image and element mapping images of ZCO/rGO hybrid composites. Scale bar, 100 nm; (b) EDS microanalysis of selected ZCO/rGO hybrid composites, the Pt signal comes from the SEM substrate.

600 nm approximately, and ZCO sphere is encapsulated in graphene. The disorder and intimate between ZCO particles and graphene sheets may restrain the agglomeration of ZCO particles, the 3D interconnected graphene conductive network may alleviate the volumetric expansion during charge/discharge process conversely. Furthermore, compared with the conventional mechanical mixed TMOs-G composites, graphene situate in microsphere ZCO particles which can provide an extra transmission channel of Li+ and electrons in sphere. Overall, microsphere ZCO/rGO hybrid composites may display an outstanding electrochemical performance. [45-47]

The microstructures of ZCO/rGO hybrid composites are further studied by TEM. As shown in Fig. 3d, graphene sheets exhibit a thin film-like with disordered and high transparency, which are the typical characteristics of theoretical structure of graphene sheets.[45,47] ZCO particles are randomly adherent to the surface of graphene sheets with a size range from 340 nm to 520 nm, which is in agreement with the above SEM observation. Fig. 3e shows the microstructure of mechanical mixed ZCO-G composites by TEM, the irregularity and transparent graphene sheets wrapped ZCO microsphere, ZCO particle size is between 580 nm and 960 nm. The high resolution TEM (HR-TEM) image (Fig. 3f) displays that the crystalline $ZnCo_2O_4$ particles are well dispersed. Besides, high crystallization and no obvious aggregation can also be observed. ZCO particles are well attached to graphene sheets, even after strong ultra-sonication for 30 min to disperse the sample for TEM characterization, suggesting strong chemical bond connection between ZCO particles and graphene sheets. The distance between adjacent lattice fringes is equal to the inter-planar distance of 1.28 Å, 1.17 Å, 2.86 Å and 2.46 Å, corresponding well to the d-value between (620) planes, (444) planes, (220) planes and (311) planes of cubic spinel $ZnCo_2O_4$, which are well consistent with the above XRD pattern. The SAED pattern (inset in Fig.3f) reveals a set of well-resolved concentric rings, representing the obtained ZCO particles in ZCO/rGO hybrid composites are polycrystalline.

The marked diffraction rings is in accordance with the (111), (311), (222) and (400) Miller indices, respectively.[45-46,48] The presence of elements in ZCO/rGO hybrid composites is confined with randomly selected areas by elemental mapping analysis in Fig. 4a. The homogeneous distribution of C, O, Co and Zn is experimentally mapped out. A shape of Co detection emerges at the same time where Zn is detected, C and O is also like this, which can be ascribed to the homogeneous combination of ZCO and graphene. The element mapping indicates that the well dispersed ZCO particles are uniformly encapsulated on graphene sheets, graphene develop twine and penetrate around ZCO microsphere to form a conductive network in ZCO/rGO hybrid composites. This special structure of graphene provide a transmission channel, relating to the interaction of $Li^+$ and inner ZCO crystals as well as the electron transfer in ZCO microsphere. What's more, the incorporate structure is beneficial to the structural stability of composites, alleviating the problem of heterogeneous electrical conductivity during delithiation process.[46-48] Fig. 4b shows the energy dispersive spectroscopy (EDS) of ZCO/rGO hybrid composites. It can be seen that the strong peaks for few elements such as C, O, Zn and Co are displayed in ZCO/rGO hybrid composites, indicating that ZCO/rGO hybrid composites are relatively bare ZCO and graphene, the amount of impurities is negligible, and the atomic ratio of Co and Zn is about 1.71:1.

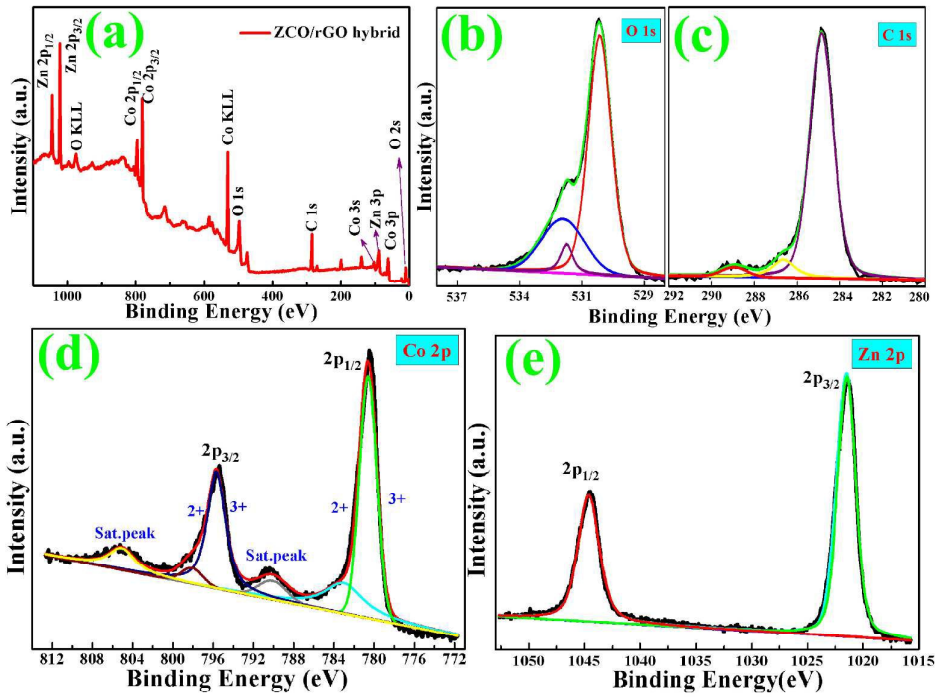


**Fig. 5.** XPS spectra of ZCO/rGO hybrid composites: (a) survey spectrum; (b) O 1s region; (c) C 1s region; (d) Co 2p region; (e) Zn 2p region.

In order to further characterize the element composition and the chemical state of ZCO/rGO hybrid composites, all of the binding energies obtained in the XPS analysis are corrected for specimen charging by reference the C 1s peak to 284.6 eV, and the results are presented in Fig. 5. Fig. 5a gives the full scale XPS spectrum of ZCO/rGO hybrids composites in the region of 0-1100 eV. The results clearly illustrate the presence of Zn atom, Co atom, C atom and O atom in the testing sample that are absence of other impurities, and the peaks are attributed to the characteristic peaks of C 1s, O 1s, Co 2p and Zn 2p, respectively. Fig. 5b displays the O 2p region, and the O 1s emission spectrum can be divided into two main peaks. The binding energy of 530.43 eV is typical of metal-oxygen (Zn-O and Co-O). 532.12 eV and 533.54 eV are attributed to the residual oxygen-containing groups, such as C-O, O-H and O=C-O, which are located on the surface of graphene sheets.[49] Fig. 5c shows the high-resolution C 1s region, which is further separated into three peaks at 285.34 eV, 287.52 eV and 289.36 eV, corresponding to the C-C, C-O, C=O and O=C-O groups, respectively.[50-51] In conclusion, the analysis of C 1s region and O 1s region suggests that few residual oxygen containing functional groups exist in the surface of graphene sheets, for instance, including some few carboxyl groups, hydroxyl groups and extremely few absorbed water exist on the surface of rGO nanosheets.[49-51]

Fig. 5d and Fig. 5e depict a high-resolution XPS spectrum of Co 2p and Zn 2p. The Zn 2p region contains two major peaks situated at 1022.67 eV and 1044.56 eV, which are ascribed to Zn $2p_{3/2}$ and Zn $2p_{1/2}$ orbits of $Zn^{2+}$. The Co 2p region at 781.72 eV and 798.48 eV can be assigned to Co $2p_{3/2}$ and Co $2p_{1/2}$ orbits. It is noted that the spin orbit splitting of the two peaks is above 16.76 eV, which is in agreement with the reported literature.[52] What's more, two accompanied weak and shake-up satellite peaks are appreciable at 791.56 eV and 803.87 eV and the gap between the main peaks and the satellite peaks is around 12.31 eV, which indicate that the Co cation valence can be ascribed to a value of $Co^{3+}$. Those results reveal that the Zn cation exist in $Zn^{2+}$ state and Co cation exist in $Co^{3+}$ state in ZCO/rGO hybrid composites, which is well consistent with the FT-IR analysis of ZCO/rGO hybrid composites.[52-54] In addition, the ratio of Zn atomic and Co atomic in ZCO/rGO hybrid composites is calculated by the area of deconvoluted peaks and the proportion is about 1:2.

**Electrochemical properties of ZCO/rGO hybrid composites.**

Cyclic voltammetry measurements are conducted in order to investigate the redox reaction during charge/discharge process. Fig.6a shows the first five cyclic voltammograms (CV) of ZCO/rGO hybrid electrodes. According to the previous studies,[55-58] and the electrochemical reaction mechanisms of $ZnCo_2O_4$ electrodes can be comprehensively described as the following conversion reactions:

$$ZnCo_2O_4 + 8Li^+ + 8e^- \rightarrow Zn + 2Co + 4Li_2O \quad (1)$$

$$Zn + Li^+ + e^- \leftrightarrow LiZn \quad (2)$$

$$Zn + Li_2O \leftrightarrow ZnO + 2Li^+ + 2e^- \quad (3)$$

$$Co + Li_2O \leftrightarrow CoO + 2Li^+ + 2e^- \quad (4)$$

$$3CoO + Li_2O \leftrightarrow Co_3O_4 + 2Li^+ + 2e^- \quad (5)$$

In the first cycle, a sharp reduction peak is located at around 0.68 V in the cathodic process, which is ascribed to the formation of $Li_2O$ and the reduction $ZnCo_2O_4$ to $Co^0$ and $Zn^0$ as described in Equation (1), continuously accompanied by the partially irreversible decomposition of the electrolyte to form a solid electrolyte interphase film (SEI).[54] In the anodic part of the first cycle, two broad oxidation peaks at 1.84 V and 2.14 V can be associated with the oxidation of $Zn^0$ to $Zn^{2+}$ and $Co^0$ to $Co^{3+}$ shown in Equations (3)-(5).[56-57,59]

In the following 2nd, 3th, 4th and 5th cycle, it can be seen that the cathodic peak gradually moves to 0.89 V, meanwhile, it becomes broader, indicating that different electrochemical mechanisms control the two process (the formation of SEI film and irreversible reaction). However, during the subsequent charging cycles, the closed areas are almost equivalent, implying good capacity retention after the first charge/discharge process of ZCO/rGO hybrid electrodes. What's more, the special and discriminable oxidation peak at 0.21 V is demonstrating that graphene sheets in ZCO/rGO hybrid electrode can be due to the insertion of $Li^+$ into graphene sheets ($C + x\ Li^+ + e^- \leftrightarrow Li_xC$),[60] graphene sheets may hinder the movement of $Li^+$, such as disordered and wrinkled, thus impacting the reaction of $Li^+$ and $ZnCo_2O_4$ crystal.[61-62]

Fig. 6c shows the 20th and the 100th charge/discharge curves for pure ZCO electrodes, mechanical mixed ZCO-G electrodes and ZCO/rGO hybrid electrodes. In the 20th cycle, the charge/discharge capacity is 768.3/774.9 mAh $g^{-1}$ for ZCO/rGO hybrid electrodes, 704.4/709.5 mAh $g^{-1}$ for mechanical mixed ZCO-G electrodes and 285.1/286.9 mAh $g^{-1}$ for ZCO electrodes. 875.9/883.7 mAh $g^{-1}$ for ZCO/rGO hybrid electrodes, 542.9/550.7 mAh $g^{-1}$ for mechanical mixed ZCO-G electrodes and 265.7/267.9 mAh $g^{-1}$ for ZCO

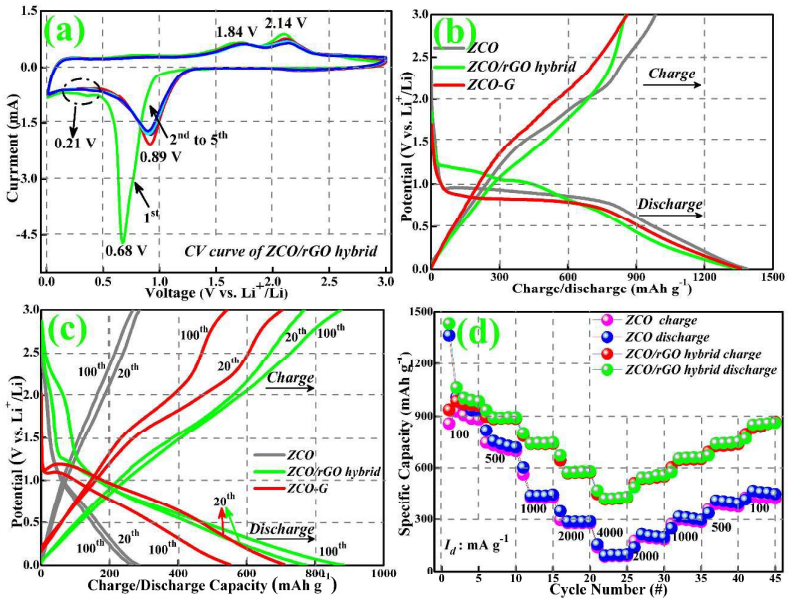


**Fig. 6.** (a) Typical CV curves of ZCO/rGO hybrid electrodes; (b) The initial charge/discharge voltage profiles of ZCO electrodes, mechanical mixed ZCO-G electrodes and ZCO/rGO hybrid electrodes at 100 mA $g^{-1}$; (c) The 20th and the 100th charge/discharge voltage profile of three electrodes at 1000 mA $g^{-1}$. (d) Rate performance of ZCO electrodes and ZCO/rGO hybrid electrodes at various current density between 100 and 4000 mA $g^{-1}$.

also act as active anode for lithium-ion batteries.

Fig.6b displays the initial charge/discharge curve of three electrodes (100 mA $g^{-1}$ in the initial four cycles and 1000 mA $g^{-1}$ at the following cycles). All electrodes exhibit large distinct plateaus between 0.9 V and 1.2 V, followed by a slope decrease to the cut off potential of 0.01 V, corresponding to the reduction of $ZnCo_2O_4$ to $Zn^0$ and $Co^0$, subsequently followed by the alloying of $Zn^0$ with $Li^0$ to LiZn, which is well consistent with CV results. The initial charge/discharge specific capacity of ZCO/rGO hybrid electrodes is 853.5/1362.3 mAh $g^{-1}$, with a coulombic efficiency of 62.65%, while 853.3/1358.6 mAh g for the mechanical mixed ZCO-G electrodes with a coulombic efficiency of 62.81% and 984.8/1388.7 mAh $g^{-1}$ for pure ZCO electrodes with a coulombic efficiency of 70.92%, and the initial charge/discharge property and coulombic efficiency of ZCO/RGO hybrid electrodes is inferior to mechanical mixed ZCO-G electrodes. Furthermore, the irreversibility capacity loss is a commonplace for high specific capacity graphene-based materials, which can be assigned to the formation of the SEI film on the surface of electrodes and the formation of $Li_2O$. Meanwhile, the initial capacity of pure ZCO electrodes is higher than that of ZCO/rGO hybrid electrodes and mechanical mixed ZCO-G electrodes. We can explain it as the primary reaction activity of graphene sheets which are not be activated completely, which is mainly because the specific structure of electrodes at the 100th cycle. It can be noted that ZCO electrodes suffer from a rapid capacity fading ranging from 1st to 20th at the high current density (1000 mA $g^{-1}$), along with a great voltage change profile, showing its poor capacity retention and electrode polarization during cycling. However, ZCO/rGO hybrid electrodes display high capacity with a mild loss and good reversibility which is better than mechanical mixed ZCO-G electrodes, the results can be assigned to the relation bonds between $ZnCo_2O_4$ and graphene sheet in electrodes, electric transmission through the interconnected graphene conductive network react with the inner $ZnCo_2O_4$ crystal and then to maintain high capacity. Afterwards, the uniform and continuous carbon buffering

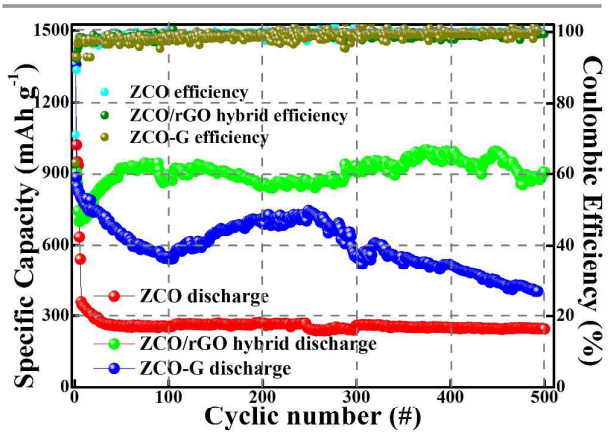


**Fig. 7.** Cyclic performance and the corresponding coulombic efficiency of ZCO electrodes, mechanical mixed ZCO-G electrodes and ZCO/rGO hybrid electrodes at 100 mA $g^{-1}$ (the initial four cycles) and 1000 mA $g^{-1}$ (the residual following cycles).

matrix can effectively alleviate volume expansion/contraction during cycling, which can significantly improve the electrochemical performance.[63-65]

electrodes. Then ZCO/rGO hybrid electrodes deliver high reversible capacity (721.4 mAh $g^{-1}$ in the 10th cycle and 883.7 mAh $g^{-1}$ in the 100th cycle). Those

**Table 1 Summarization of the reported electrochemical performance with different morphology of $ZnCo_2O_4$.**

| Element materials | Current density (mA $g^{-1}$) | Reversible capacity (mAh $g^{-1}$) | Cyclic number (#) | Reference |
|---|---|---|---|---|
| Flaked ZCO porous nanostructure | 100 | 1275 | 50 | 63 |
| Ultrathin ZCO nanosheets | 200 | 930 | 200 | 64 |
| Multimodal porous ZCO microsphere | 1000 | 856 | 1000 | 65 |
| Pineapple-shaped ZCO microspheres | 100 | 1130 | 120 | 71 |
| Mesoporous ZCO coated with Polypyrrole | 200 | 458 | 100 | 72 |
| Controllable interior structure of ZCO microspheres | 400 | 835 | 50 | 73 |
| ZCO/nitrogen-doped graphene nanostructure | 100 | 930 | 30 | 74 |
| Nano-sized ZCO anchored with graphene nanosheets | 100 | 755.6 | 70 | 75 |
| Hierarchical microsphere ZCO/rGO hybrid composites | 1000 | 904.2 | 500 | our work |

**Table.1.** Summarization of the reported electrochemical performance with different morphology of $ZnCo_2O_4$.

As can be seen in Fig. 6d, ZCO/rGO hybrid electrodes also show an excellent rate performance. The rate capability is measured by a multiple-step galvanostatic strategy at various current densities between 100 mA $g^{-1}$ and 4000 mA $g^{-1}$. When checked for the different current density, which is increased from 100 to 500, 1000, 2000, and to 4000 mA $g^{-1}$, ZCO/rGO hybrid electrodes deliver a high charge/discharge capacity of 936.7/1432.5, 897/933.7, 786.8/802.4, 642.8/672.4, 448.5/469.7 mAh $g^{-1}$, respectively. In conclusion, pure ZCO electrodes show an inferior charge/discharge capacity, 857.8/1365.1, 562.5/602.7, 295.7/347.5, 139.7/155.6 mAh $g^{-1}$. When the current density is reversed back to 100 mA $g^{-1}$, the specific charge/discharge capacity of ZCO/rGO hybrid electrodes can recover a high value of 796.2/769.8 mA h $g^{-1}$, however, just 426.7/416.2 mAh $g^{-1}$ for pure ZCO electrodes. As a result, the superior rate performance can be attributed to the structure of graphene sheets in ZCO/rGO hybrid composites, which possess favorable charge/discharge transport features of the 3D structure.[27,60,66-68] The peculiar structure inhibits the volume change during the transportation of $Li^+$ and shortens the diffusion length of $Li^+$ in the thickness direction. In conclusion, the rate performance of ZCO/rGO hybrid electrodes is better than ZCO electrodes.

Fig. 7 shows the cycling performance and the coulombic efficiency of pure ZCO electrodes, mechanical mixed ZCO-G electrodes and ZCO/rGO hybrid

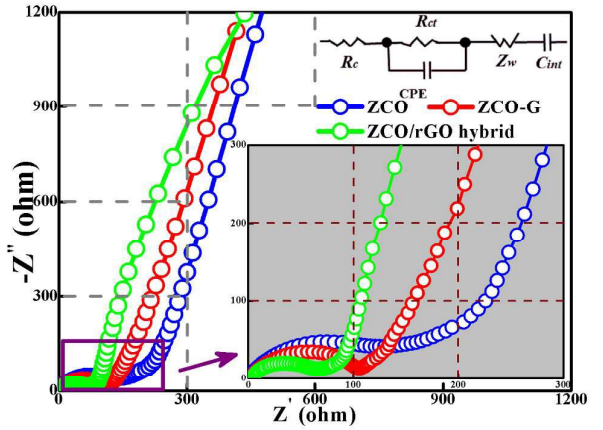


**Fig. 8.** Nyquist plots measures in the frequency for ZCO electrodes, mechanical mixed ZCO-G electrodes and ZCO/rGO hybrid electrodes.

increased capacities can be ascribed to the destruction in the graphite lattice during the insertion/extraction of $Li^+$ and the generation of more defect and active for lithium-ion storage.[65,67-69] By contrast, the capacity retention of pure ZCO electrodes is very low and has a monotonous decrease to 267.9 mAh $g^{-1}$ in the 100th cycle. Compared with ZCO/rGO hybrid electrodes, mechanical mixed ZCO/rGO electrodes display an inferior discharge capacity of 549.2 mAh $g^{-1}$ in the 100th cycle.

In the initial four cycles, the decreases of cycling stability are assigned to the partial formation and decomposition of SEI film on the surface of materials. In the following cycles, the coulombic efficiencies of three electrodes exceed 95%, which are consistent with the above-mentioned analysis.[70-72] Furthermore, ZCO/rGO hybrid electrodes display high reversible cyclic performance during the following 50 cycles, however, pure ZCO electrodes suffer from rapid capacity fading. After 500 cycles, the discharge capacity of ZCO/rGO hybrid electrodes maintain at 904.2 mAh $g^{-1}$ with a capacity retention of 66.4%, which is much higher than that of ZCO electrodes (244.4 mAh $g^{-1}$ with the capacity retention of 17.6%) and mechanical mixed ZCO-G electrodes ( 402.5 mAh $g^{-1}$ with the capacity retention of 29.5%). Therefore, we can infer that the existence of graphene alleviate the volumetric expansion and provides the superior electron conductivity, which can hinder the aggregation of $ZnCo_2O_4$ particles and electrode cracking during the cyclic process. Herein, interconnected graphene conductive network acts as the special channels between individual components of the active materials and the current collectors.[68,73-76] In addition, the summarization of the reported electrochemical performance of $ZnCo_2O_4$ with different morphology is shown in Table 1. It can be obviously seen that hierarchical microsphere ZCO/rGO hybrid electrodes have the most excellent cyclic performance when compared to the other ZCO electrodes in Table 1, whatever method and morphology ZCO is synthesized. It can be seen from the Table.1 that both preparing special morphology ZCO and compositing with other materials, those materials show a high electrochemical performance under the low current densities at the initial electrochemical cyclic performance. By

contrast, ZCO/RGO hybrid composites display a better excellent electrochemical performance under the above condition via a polyol process.

Electrochemical impedance spectroscopy (EIS) is carried out to evaluate the resistance against electron transfer and the impedance of the electrodes during cycling. Fig. 8 shows three Nyquist plots consisting of a single semicircle and an inclined line. The semicircle in medium-high frequency region is characteristic of charge transfer resistance (electrolyte resistance and surface film resistance) and the linear line at approximately 45˚ in low frequency region represents the Warburg impedance, which is ascribed to solid state diffusion of $Li^+$ through the bulk of the active materials.[77] The inset in Fig. 8 shows the equivalent circuit. Hence, the circuit elements consist of the ohmic resistance ($R_e$), charge transfer resistance ($R_{ct}$), a constant phase element (CPE) corresponding to the double layer capacitance ($C_{dl}$) and the surface film capacitance ($C_{sf}$), and the Warburg impedance ($Z_w$) which is related to the solid state diffusion of $Li^+$ in the electrodes.[70,77-78] The charge transfer resistance $R_{ct}$ of ZCO/rGO hybrid electrodes (65.8 **Ω**) is significantly smaller than that of mechanical mixed ZCO-G electrodes (114.3 **Ω**) and ZCO electrodes (152.6 **Ω**), indicating that the existence of graphene sheets in the ZCO/rGO hybrid electrodes generate a more stable surface film (including the SEI film) and the higher electron conductivity compared with that of ZCO electrodes and mechanical mixed ZCO-G electrodes. The results indicate that the electron transfer and $Li^+$ diffusion of ZCO/rGO hybrid electrodes are much faster than that of ZCO electrodes and mechanical mixed ZCO-G electrodes during charge/discharge process and then generate outstanding electrochemical rate capability. Those above-mentioned analysis manifest that the electrochemical performance of ZCO/rGO hybrid electrodes are much better than that of ZCO electrodes and mechanical mixed ZCO-G electrodes.

The SEM images of pure ZCO electrodes, mechanical mixed ZCO-G electrodes and ZCO/rGO hybrid electrodes after 100 cycles of charge/discharge process at 1000 mA $g^{-1}$ is applied to further differentiate the electrochemical behavior during cycling in Fig. 9. According to the previous works, all the cracks in SEM images can be ascribed to the repeated volume change by conversion reaction between metal atomic and metal oxides. As can be shown in Fig. 9a&b, the micro-structure of pure ZCO electrodes is destroyed completely during charge/discharge process. ZCO particles display agglomeration severely and much more cracks of large volume expansion for the formation of SEI film, and the crack size is range from 600 nm to 800 nm. Besides, some nano-sized pores on the surface of electrodes are due to a volume change (marked with yellow arrows), but those cracks and pores will diminish in the effective contact areas between the electrolyte and active materials.

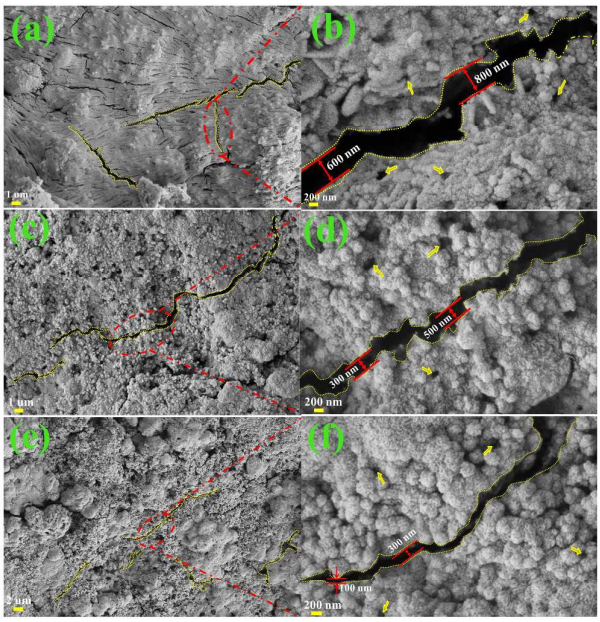


**Fig. 9.** Typical SEM images of pure ZCO electrodes (a&b), mechanical mixed ZCO-G electrodes (c&d) and ZCO/rGO hybrid electrodes (e&f) after 100 cycles of charge/discharge process at a current density of 1000 mA $g^{-1}$, respectively.

The SEM images of mechanical mixed ZCO-G electrodes and ZCO/rGO hybrid electrodes after cycling are also displayed in Fig. 9c&d and Fig. 9e&f. Several narrow cracks and nano-sized pores are presented on the surface of mechanical mixed ZCO-G electrodes and ZCO/rGO hybrid electrodes due to a slight volume expansion (the crack size is between 300 nm and 500 nm, 100 nm and 300 nm, respectively). Owing to the existence of graphene sheets in active electrodes, in comparison to pure ZCO electrodes, the texture of two electrodes can be well retained and the surface of the electrodes is smooth except some tiny cracks and pores, which will not greatly impact on the insertion/extraction of $Li^+$. So a certain amount existence of graphene sheets which are composited in active electrodes can improve the electrochemical performance to a great extent.

## Conclusions

In summary, we have synthesized a chemically integrated hierarchical microsphere $ZnCo_2O_4$/graphene hybrid structure through a polyol path. ZCO particles embedded in graphene sheets and then graphene grew and interwoven as a conductive network basic skeleton in the inside of microsphere $ZnCo_2O_4$ particles in inverse, owing to the excellent features of this 3D structure ZCO/rGO hybrid composites exhibit large discharge capacity (1362.3 mAh $g^{-1}$ at the initial cycle), high rate capacity (469.7 mAh $g^{-1}$ at the current density of 4 A $g^{-1}$), and outstanding cycling performance (904.2 mAh $g^{-1}$ after 500 cycles at the current density of 1 A $g^{-1}$). Consequently, these rationally syntheses of ZCO/rGO hybrid composites make it a promising candidate as a superior anode materials for lithium-ion batteries.

## Experimental

All the reagents are analytically grade, commercially available and used without further purification.

### Preparation of graphene oxide (GO)

GO employed here was synthesized from natural flake graphite by a novel modified Hummers method. Firstly, 1 g natural graphite powders were added into 23 mL of 98 wt% $H_2SO_4$ aqueous solution (Aladdin, 99%) and 10 mL of 98 wt% $HNO_3$ aqueous solution (Aladdin, 99%), with vigorous stirring for 1 h in ice bath, keeping temperature at 0 ˚C. Subsequently, 4 g $KMnO_4$ (Aladdin, 98%) was added gradually under continuously stirring, the temperature of the mixed solution don't exceed 15 ˚C. After being continuously reacted for 40 min at 35 ˚C, 70 mL deionized water and 8 mL 10 wt.% $H_2O_2$ aqueous solution were added dropwise into the solution accompanied with the change of the solution color to golden yellow, and then continuously reated for another 15 min under strong magnetic stirring. Later, the mixture was centrifuged (8000 rpm) and washed with 80 mL of 5 wt.% HCl aqueous solution (Aladdin, 99 %) for two times, deionized water and absolute ethanol for several times. Finally, the resultant solution was collected and dried at 60 ˚C in vacuum, GO is obtained.

### Preparation of ZCO/rGO hybrid composites

ZCO/rGO hybrid composites were synthesized by using a polyol process. Firstly, 60 mg dried GO was added into 65 mL of ethylene glycol (Aladdin, 99%) under vigorous ultrasonic treatment for 1 h to form a homogeneous solution. Meanwhile, 0.110 g $Zn(Ac)_2 \cdot 2H_2O$ (Aladdin, 99%) and 0.249 g $Co(Ac)_2 \cdot 4H_2O$ (Aladdin, 99%) were dissolved in 35 mL ethylene glycol under vigorous stirring. The above two systems were then mixed together and stirred for 45 min. The obtained solution was transferred into a round bottom flask and heated to 180 °C in an oil bath. After refluxing for 12 h, the solution was cooled down to room temperature naturally. Finally, the precipitate was collected by centrifugation and washed with ethanol for four times. The precipitate was then annealed at 200 °C in air for 2 h with a heating rate of 0.5 °C $min^{-1}$ to get ZCO/rGO hybrid composites. For comparison, we have prepared bare $ZnCo_2O_4$ (ZCO) materials by adopting the same typical synthesis as the above mentioned, 0.110 g $Zn(Ac)_2 \cdot 2H_2O$ and 0.249 g $Co(Ac)_2 \cdot 4H_2O$ were dissolved in 100 mL ethylene glycol were used for the reaction. The mechanical mixed bare $ZnCo_2O_4$ and graphene sheets in order to obtain $ZnCo_2O_4$-Graphene (ZCO-G) composites under the identical condition.

**Material characterization**

The crystal structures and morphology of ZCO/rGO hybrid composites were checked by X-ray diffraction employing a scanning rate of 0.033° $s^{-1}$ in a 2θ range from 10° to 85° (XRD; PANalytical X'Pert PRO, CuKα radiation, λ=0.15406 nm), scanning electron microscopy (SEM; ZEISS ULTRA 55) and transmission electron microscopy (TEM; JEM-2100 HR). Thermogravimetric analysis (TGA, PerkinElemer, Inc; USA) are conducted from the room temperature to 680 ºC in air at the heating rate of 10 °C $min^{-1}$. Fourier transform infrared spectroscopy (FT-IR) was recorded with the wave from 4000 to 400 $cm^{-1}$ (WQF-410, Beijing Secondary Optical Instruments; China). Raman spectroscopy measurement was carried out on a Labor Raman HR-800 Raman spectrometer system with the wave of 1000 $cm^{-1}$ to 3200 $cm^{-1}$, with a 632.8 nm wavelength laser light. Surface analysis of samples are carried out with X-ray photoelectron spectrum (XPS, ESCALAB 250 with 150 W Al Ka probe beam), all binding energies are referenced to the C 1s peak (284.6 eV).

**Electrochemical measurements**

The electrochemical performance was tested by using half-cells (CR2430). Working electrode was made by mixing 80 wt% active materials (ZCO/rGO hybrid composites and mechanical mixed ZCO-G composites in synthesized sample, bare ZCO materials in control sample), 10 wt% acetylene black as conducting agent and 10 wt% LA132 as binder. The working electrode slurry was well dispersed via coating machine and fabricated on the copper foils of 13 μm thickness and dried at 80 ˚C for 12 h under vacuum. The electrode was pressed and punched. CR2430 button cells were assembled in an argon-filled glove box. The electrolyte was 1.0 M $LiPF_6$ in a mixture of ethylene carbonate (EC), diethyl carbonate (DEC), and ethyl methyl carbonate (EMC) (1:1:1 by volume, provided by Chei Industries Inc, South Korea). The separator was made of a Celgard 2400 film. The charge/discharge test was conducted at 100 mA $g^{-1}$ for galvanostatic measurements in 0.01 V and 3.0 V (vs. $Li^+$/Li) by NEWARE Battery Test System and LAND Battery Test System. The cyclic voltammogram was performed at a scan rate of 0.2 mV $s^{-1}$ between 0.01 V and 3.00 V, and the impedance analysis was carried out by CHI604D Electrochemistry System with a frequency range of 100 kHz - 0.01 Hz. All of the electrochemical measurements were carried out at 25 ˚C.

## Acknowledgements

This work was supported by the National Natural Science Foundation of China (Grant No. 51101062 and 51171065), The Natural Science Foundation of Guangdong Province (No.S2010020010937).The Project Supported by Guangdong Natural Science Foundation(No. 2014A030313436) and the Foundation for Distinguished Young Talents in Higher Education of Guangdong, China (Grant No. LYM09052).

## References

[1] J. B. Goodenough and K. S. Park, J. Am. Chem. Soc., 2013, **135**, 1167.
[2] M. Armand, J.M. Tarascon, Nature, 2008, **451**, 652.
[3] G. Wang, H. Liu, J. Liu, S. Qiao, G. M. Lu, P. Munroe and H. Ahn, Adv. Mater., 2010, **22**, 4944.
[4] Y.W. Zhu, S. Murali, M.D. Stoller, K.J. Ganesh, W.W. Cai, P.J. Ferreira, A. Prikle, R. M. Wallace, K.A. Cychosz and M. Thommes, Science, 2011, **332**, 6037.
[5] J. Chen, L. N. Xu, W.Y. Li, X.L. Gou, Adv. Mater., 2005, **17**, 582.
[6] X. Gu, L. Chen, S. Liu, H.Y. Xu, J. Yang, Y.T. Qian, J. Mater. Chem. A, 2014, **2**, 3439.
[7] K. Xie, J. Li, Y. Q. Lai, W. Lu, Z. Zhang, Y. X. Liu, L. Zhou and H. T. Huang, Electrochem. Commun., 2011, **2**, 657.
[8] J. W. Lee, T. Ahn, J. H. Kim, J. M. Ko and M. D. Kim, Electrochim. Acta, 2011, **56**, 4849.
[9] B. Varghese, M. V. Reddy, Y. W. Zhu, C. S. Lit, T. C. Hoong, G. V. S. Rao, B. V. R. Chowdari, A. T. S. Wee, C. T. Lim, C. H. Sow, Chem. Mater., 2008, **20**, 3360.
[10] J. J. Zhang, J. W. Liang, Y. C. Zhu, D. H. Wei, L. Fan, Y. T. Qian, J. Mater. Chem. A, 2014, **2**, 2728.
[11] C. Chen, Q. Ru, B.N. An, X. Song, X. H. Hou, Electrochim. Acta, 2015, **15**, 203.
[12] G. Q. Zhang, L. Yu, H. B. Wu, H. E. Hoster, X. W. Lou, Adv. Mater., 2012, **24**, 4609.
[13] W. P. Kang, Y. B. Tang, W. Y. Li, Z. P. Li, X. Yang, J. Xu, C. S. Lee, Nanoscale, 2014, **6**, 6551.
[14] B. Liu, J. Zhang, X. Wang, G. Chen, D. Chen, C. Zhou and G. Shen, Nano Lett., 2012, **12**, 3005.
[15] C. Fu, G. Li, D. Luo, X. Huang, J. Zheng and L. Li, ACS Appl.Mater. Interfaces, 2014, **6**, 2439.
[16] H. Zhang, H. Li, H. Wang, K. He, S. Wang, Y. Tang and J. Chen, J. Power Sources, 2015, **280**, 640.
[17] M.V. Reddy, G.V.S. Rao, B.V.R. Chowdari, Chem. Rev., 2013,**113**, 5364.
[18] K.S. Novoselov, A.K. Geim, S.V. Morozov, D. Jiang, Y. Zhang, S.V. Dubonos, I.V. Grigorieva, A.A. Firsov, Science, 2004, **306**, 666.
[19] A. K. Geim, Science, 2009, **324**, 1530.
[20] Y. Q. Sun, Q. Wu, G. Q. Shi, Energ. Environ. Sci., 2011, **4**, 1113.
[21] N. Tombros, C. Jozsa, M. Popinciuc, H. T. Jonkman, B. J. Vanwees, Nature, 2007, **448**, 571.
[22] M. Q. Li, Y. Yu, J. Li, B. L. Chen, A. Konarov, P. Chen, J. Power Source, 2015, **293**, 976.

[23] Y. Huang, J. J. Liang, Y. S. Chen, Small, 2012, **8**, 1805.

[24] J. X. Zhu, T. Zhu, X. Z. Zhou, Y. Y. Zhang, X. W. Lou, X. D. Chen, H. Zhang, H. H. Hng, Q. Y. Yan, Nanoscale, 2011, **3**, 1084.

[25] S. P. Wu, R. Xu, M. J. Lu, R. Y. Ge, I. James, C. P. Han, B. B. Zhang, Z. Q. Lin, Adv. Energy. Mater., 2015, **1504**, 1.

[26] B. Liu, J. Zhang, X. F. Wang, G. Chen, D. Chen, C. W. Zhou, G. Z. Shen, Nano Lett., 2012, **12**, 3005.

[27] Y. Sharma, N. Sharma. G. V. S. Rao, B. V. R. Chowdari, Adv. Funct. Mater., 2007, **17**, 2855.

[28] Y. Q. Zhu, C. B. Cao, J. T. Zhang, X. Y. Xu, J. Mater. Chem. A, 2015, **3**, 9556.

[29] H. W. Liu, J. Wang, Electrochim. Acta, 2013, **92**, 371.

[30] S. J. Hao, B. W. Zhang, S. Ball, M. Copley, Z. C. Xu, M. Srinivasan, K. Zhou, S. Mhaisalkar, Y. Z. Huang, J. Power Source, 2015, **294**, 112.

[31] R. Wu, X. Qian, K. Zhou, J. Wei, J. Lou and P. M. Ajayan, ACS NANO, 2014, **8**, 6297.

[32] X. Zhou, W. Feng, C.Wang, X. L. Hu, X. W. Li, P. Sun, K. Shimanoe, N. Yanmazoe, G. Y. Lu, J. Mater. Chem. A, 2014, **2**, 17683.

[33] S. Park, J. An, J. R. Potts, A. Valamakanni, S. Murali, R. S. Ruoff, Carbon, 2011, **49**, 3019.

[34] N.R. Tao, M.L. Sui, J. Lu, K. Lu, Nano Struct. Mater., 1999, **11**, 433.

[35] H. W. Zhang, Z. K. Hei, G. Liu, J. Lu, K. Lu, Acta Mater., 2003, **51**, 1871.

[36] S. Stankovich, R. D. Piner, S. T. Nguyen, R. S. Ruoff, Carbon, 2006, **44**, 3342.

[37] G. M. Scheuermann, L. Rumi, P. Steurer, W. Bannwarth, R. Mulhaupt, J. Am. Chem. Soc., 2009, **131**, 8262.

[38] M. Imran, D. H. Kim, W. A. Aimasry, A. Mahmood, A. Hassan, S. Haider, S. M. Ramay, Polym. Degrad. Stabil.,2013, **98**, 904.

[39] T. L. Phan, N. X. Nghia, S. C. Yu, Solid. State. Commun., 2012, **152**, 2087.

[40] S. J. Deng, R. Han, C. J. Dong, X. C. Xiao, J. M. Wu, Y. D. Wang, 2014, **134**, 138.

[41] C. N. R. Rao, A. K. Sood, K. S. Subramanyam, A. Govindaraj, Angew. Chem. Int. Edit., 2009, **48**, 7752.

[42] S. Stankovich, D. A. Dikin, R. D. Piner, K. A. Kohlhaas, A. Kleinhammes, Y. Jia, Y. Wu, S. T. Nguyen, R. S. Ruoff, Carbon, 2007, **45**, 1558.

[43] K. N. Kudin, B. Ozbas, H. C. Schniepp, R. K. Prud, I. A. Aksay, R. Car, Nano Lett., 2008, **8**, 36.

[44] G. X. Wang, J. Yang, J. Park, X. L. Gou, B. Wang, H. Liu, J. Yao, J. Phys. Chem. C, 2008, **112**, 8192.

[45] H. Wang, H.B. Feng, J.H. Li, Small, 2014, **11**, 2165.

[46] P.C. Lian, X.F. Zhu, S.Z. Liang, Z. Li, W.S. Yang, H.H. Wang, Electrochim. Acta., 2010, **55**, 3909.

[47] M. Lotya, P. J. King, U. Khan, S. De, J. N. Coleman, ACS NANO, 2010, **4**, 3155.

[48] X. H. Wei, D. H. Chen, W. J. Tang, Mater. Chem. Phys., 2007, **103**, 54.

[49] S. Park, J. An, J. R. Potts, A. Velamakanni, S. Murali, R. S. Ruoff, Carbon, 2011, 49, 3019.

[50] X. L. Li, H. L. Wang, J. T. Robinson, H. Sanchez, G. Diankov, H. J. Dai, J. Am. Chem. Soc., 2009, **131**, 15939.

[51] L. H. Tang, Y. Wang, Y. M. Li, H. B. Feng, J. Lu, J. H. Li, Adv. Funct. Mater., 2009, 19, 2782.

[52] L. L. Hu, B. H. Qu, C. C. Li, Y. J. Chen, L. Mei, D. N. Lei, L. B. Chen, Q. H. Li, T. H. Wang, J. Mater. Chem. A, 2013, **1**, 5596.

[53] H. X. Guo, J. H. Chen, W. Weng, Q. X. Wang, S. X. Li, Biochem. Eng. J., 2014, **239**, 192.

[54] Y.C. Qiu, S.H. Yang, H. Deng, L.M. Jin, W.S. Li, J. Mater. Chem. A, 2014, **20**, 4439.

[55] L. Huang, G.H. Waller, Y. Ding, D.C. Chen, D. Ding, P.X. Xi, Z.L. Wang, M.L. Liu, Nano Energy, 2015, **11**, 64.

[56] T. Y. Wei, C. H. Chen, H. C. Chien, S. Y. Lu, C. C. Hu, Adv. Mater., 2010, **20**, 347.

[57] Q. Xie, F. Li, H. Guo, L. Wang, Y. Chen, G. Yue, D. L. Peng, ACS Appl. Mater. Interfaces, 2013, **5**, 5508.

[58] W. Luo, X.L. Hu, Y.M. Sun, Y.H. Huang, J. Mater. Chem., 2012, **22**, 8916.

[59] C. E. Banks, T. J. Davies, G. G. Wildgoose, R. G. Compton, Chem. Commun., 2005, **7**, 829.

[60] Z.S. Wu, W.C. Ren, L. Wen, L.B. Gao, J.P. Zhao, Z.P. Chen, G.M. Zhou, F. Li, H.M. Cheng, ACS NANO, 2010, **4**, 3187.

[61] G. Wang, X.P. Gao, P.W. Shen, J. Power Sources, 2009, **192**, 719.

[62] W. M. Zhang, X. L. Wu, J. S. Hu, Y. G. Guo, L. J. Wan, Adv. Funct. Mater., 2008, **18**, 3941.

[63] A. L. M. Reddy, M. M. Shaijumon, S. R. Gowda, P. M. Ajayan, Nano Lett., 2009, **9**, 1002.

[64] J. L. Zhu, Y. Y. Li, S. Kang, X. L. Wei, P. K. Shen, J. Mater. Chem. A, 2015, **2**, 3142.

[65] X. J. Zhu, Y. W. Zhu, S. Maurali, M. D. Stollers, R. S. Ruoff, ACS NANO, 2011, **5**, 3333.

[66] Z. S. Wu, G. M. Zhou, L. C. Yin, W. Ren, F. Li, H. M. Cheng, NANO Energy, 2012, **1**, 107.

[67] X. S. Zhou, L. J. Wan, Y. G. Guo, Adv. Mater., 2013, **5**, 2152.

[68] X. Song, Q. Ru, B. B. Zhang, S. J. Hu, B. N. An, J. Alloy. Compd., 2014, **58**, 518.

[69] Y. Q. Zhu, C. B. Cao, J. T. Zhang, X. Y. Xu, J. Mater. Chem. A, 2015, **3**, 9556.

[70] S. J. Hao, B. W. Zhang, B. Sarah, C. Mark, Z. C. Xu, S. Madhavi, K. Zhou, M. Subodh, Y. Z. Huang, J. Power. Source, 2015, **294**, 112.

[71] L. Y. Guo, Q. Ru, X. Song, S. J. Hu, Y. D. Mo, J. Mater. Chem. A, 2015, **3**, 8683.

[72] X. B. Zhong, H. Y. Wang, Z. Z. Yang, B. Jin, Q. C. Jiang, J. Power. Sources, 2015, **296**, 298.

[73] L. Huang, H. W. Gordon, Y. Ding, D. C. Chen, P. X. Xi, Z. L. Wang, M. L. Liu, Nano. Energy, 2015, **11**, 64.

[74] S. Sahoo, S. H. Bae, Y. S. Lee, J. M. Lee, J. M. Ahn, C. G. Kim, I. K. Oh, Carbon, 2015, **94**, 455.

[75] A. K. Rai, T. V. Thi, B. J. Paul, J. Kim, Electrochim, Acta., 2014, **146**, 577.

[76] B. Jin, E.M. Jin, K.H. Park, H.B. Gu, Electrochem. Commun., 2008, **10**, 1537.

[77] G. Zhou, D. W. Wang, L. C. Yin, N. Li, F. Li and H. M. Cheng, ACS NANO, 2012, **10**, 3214.

[78] M. V. Reddy, T. Yu, C. H. Sow, Z. X. Shen, C. T. Lim, G. V. S. Rao, B. V. Chowdari, Adv. Funct. Mater., 2007, **17**, 2792.

## Graphic abstract:

$ZnCo_2O_4$/rGO hybrid composites synthesized by an alcoholization process, together with hierarchical microsphere znic cobalt oxides (ZCO) embedded in the graphene sheets, can display superior rate capability and enhanced cyclic stability during cycling.